On the applicability of cosine-modulated pulses for high-resolution solid-state NMR of quadrupolar nuclei with spin $> 3/2$.

Akiko Sasak, Julien Trebosc, Hiroki Nagashima, Jean-Paul Amoureux

On the applicability of cosine-modulated pulses for high-resolution solid-state NMR of quadrupolar nuclei with spin > 3/2

Akiko Sasaki,[a,c] Julien Trébosc,[b] Hiroki Nagashima,[c] Jean-Paul Amoureux[d,e,*]

[a.] *Bruker Japan K.K., 3-9, Moriya-cho, Kanagawa-ku, Yokohama-shi, Kanagawa 221-0022, Japan.*
[b.] *Univ. Lille, CNRS, INRAE, Centrale Lille, Univ. Artois, FR 2638 - IMEC – Institut Michel-Eugène Chevreul, F-59000 Lille, France.*
[c.] *Interdisciplinary Research Center for Catalytic Chemistry, National Institute of Advanced Industrial Science and Technology (AIST), 1-1-1 Higashi, Tsukuba, Ibaraki 305-8565, Japan.*
[d.] *Bruker Biospin, 34 rue de l'industrie, F-67166 Wissembourg, France.*
[e.] *Univ. Lille, CNRS, Centrale Lille, ENSCL, Univ. Artois, UMR 8181 – UCCS – Unit of Catalysis and Chemistry of Solids, F-59000 Lille, France.*

In MQMAS-based high-resolution solid-state NMR experiments of half-integer spin quadrupolar nuclei, the high radiofrequency (RF) field requirement for the MQ excitation and conversion steps with two hard-pulses is often a sensitivity limiting factor in many practical applications. Recently, the use of two cosine-modulated (cos) low-power (lp) pulses, lasting one-rotor period each, was successfully introduced for efficient MQ excitation and conversion of spin-3/2 nuclei with a reduced RF amplitude. In this study, we extend our previous investigations of spin-3/2 nuclei to systems with higher spin values and discuss the applicability of coslp-MQ excitation and conversion in MQMAS and MQ-HETCOR experiments under slow and fast spinning conditions. For the numerical simulations and experiments we used a moderate magnetic field of 14.1 T. Two spin-5/2 nuclei (^{85}Rb and ^{27}Al) are mainly employed with a large variety of C_Q values, but we show that the practical set up is also available for higher spin values, such as spin-9/2 with ^{93}Nb in $Cs_4Nb_{11}O_{30}$. We demonstrate for nuclei with spin value larger than 3/2 a preferential use of coslp-MQ acquisition for low-gamma nuclei and/or large C_Q values with a much reduced RF-field with respect to that of hard-pulses used with conventional methods.

I. Introduction

Despite that nuclei with spin value I > ½ account for more than 70% of NMR-active isotopes, many practical applications of these nuclei are severely limited due to the presence of the quadrupolar interactions, which cause spectral broadenings and thus result in a significant loss of sensitivity and resolution. To eliminate this broadening, which is proportional to the quadrupolar coupling constant, $C_Q = e^2qQ$, magic angle spinning (MAS)[1] is routinely employed in solid-state NMR (ssNMR). For half-integer spin quadrupolar nuclei (I = 3/2, 5/2, 7/2 and 9/2), high-resolution two-dimensional (2D) experiments, such as multiple-quantum MAS (MQMAS)[2] or satellite-transition MAS (STMAS),[3] are performed to obtain truly isotropic spectra. Although MQMAS is more widely used than STMAS as a routine method owing to its ease in experimental setup, these two methods are complementary to each other as their comparison allows to identify the potential presence of dynamics close to the quadrupolar nuclei.[4,5] Moreover, following the development of fast MAS probes with small-diameter rotors, ^{1}H-detected HETCOR (hetero-nuclear correlation) experiments with quadrupolar nuclei have been proposed,[6–13] which utilize the improved ^{1}H resolution under fast spinning.[14,15] The acquisition of MQMAS/STMAS and MQ/ST-HETCOR 2D spectra allows a detailed analysis of the local structure around the quadrupolar nuclei of interest, in much the same way that has been employed for I = 1/2 spin systems.

In the MQ-based high-resolution experiments, the intrinsically low efficiency of the MQ excitation/conversion steps is often a sensitivity-limiting factor in practical applications. This is because the coherences on the three-quantum level are 'forbidden' from the quantum mechanics point of view, and therefore the MQ excitation and conversion processes with conventional hard-pulses (hp) require a high radiofrequency (RF) field,[16] which moreover depends on the C_Q value.

Such large RFs are not always attainable, especially with low-gamma nuclei, or when large diameter rotors ($\varnothing \geq 3$mm) are used for insensitive isotopes. To circumvent this high RF requirement of the conventional hard-pulses, a variety of experimental approaches has been implemented, such as RIACT,[17] FAM,[18,19] DFS,[20] FASTER,[21] HS,[22] RAPT,[23] and QCPMG-MQMAS,[24] although they often require a time-consuming optimization process of multiple parameters.

Recently, two novel variations for MQ excitation/conversion were devised, namely lp-MQMAS[25] and coslp-MQMAS,[26] which utilize two identical low-power long-pulses (lp) of one rotor period (τ_R) each, enabling the MQ excitation/conversion with a reduced RF field. These two approaches stem from the lp-STMAS scheme,[27] previously proposed to manipulate the innermost STs with low RF requirement. In this article and in the previous one,[31] we use a notation of the sequences that slightly differs from the original ones.[25,26] We call them lp-MQMAS and coslp-MQMAS, instead of lpMQMAS and cos-lpMQMAS, to emphasize the fact that they are MQMAS methods, and we add WURST at the beginning to emphasize the fact that this sweeping is a very important part of these sequences.

In coslp-MQMAS, the amplitude of the two identical τ_R-pulses is cosine-modulated, and it has been shown that with respect to lp-MQMAS, which uses two square pulses, the efficiency is about 30% higher and the isotropic linewidths are narrower and hence more resolved owing to its robustness to spinning instability.[26] Since the lp- and coslp-MQMAS sequences begin with a central-transition (CT) selective 90° pulse, they both benefit from the existing CT signal enhancement schemes. Among those well-

established approaches, the WURST (wideband, uniform-rate, smooth-truncation)[28–30] scheme was chosen for the ease of implementation in the aforementioned lp- and coslp-MQMAS studies.[25,26]

Recently, we have made a thorough investigation on I = 3/2 nuclei of the practical aspects of MQMAS and MQ-HETCOR experiments under slow and fast MAS conditions, using ^{87}Rb, ^{71}Ga and ^{35}Cl isotopes. Our study concluded that WURST-coslp-MQ-based experiments are highly recommended for (i) low-gamma nuclei, (ii) large rotor diameters, and (iii) samples with large C_Q values.[31] For I > 3/2 spin systems, at the time of writing, only ^{17}O WURST-coslp-MQMAS results have been reported in the acquisition of 3D ^{1}H/^{13}C/^{17}O,[32] or 2D ^{1}H/^{17}O,[33] isotropic HETCOR spectra at B_0 = 18.8 T.

In this study, we extend our previous investigations of spin-3/2 nuclei to higher spin systems, mostly to I = 5/2, and discuss the applicability of coslp-MQ excitation/conversion in the context of MQMAS and MQ-HETCOR under slow and fast spinning conditions. All experiments and simulations presented in this article have used a moderate magnetic field of B_0 = 14.1 T. Two I = 5/2 isotopes, ^{85}Rb and ^{27}Al, have been employed with a large range of C_Q values. With the aid of numerical simulations, the robustness of WURST sensitivity enhancements has been verified for I = 5/2 nuclei. Using ^{85}Rb in $RbNO_3$ (C_Q = 3-4 MHz)[34,35] and Rb_2SO_4 (C_Q = 5 and 11 MHz),[36] a preferential use of WURST-coslp-MQMAS over the conventional approaches is demonstrated for low-gamma nuclei and either large C_Q values or rotor diameters. Additionally, using ^{27}Al in $AlPO_4$-berlinite (C_Q = 4 MHz),[35,37] Al(acac)$_3$ (Al acetylacetonate: C_Q = 3 MHz),[38] Al(lact)$_3$ (Al lactate: C_Q = 5 MHz),[15] and ipa-$AlPO_4$-14 (C_Q = 1.8-5.6 MHz),[5,39,40] we briefly comment on the z-filter and shifted-echo versions of coslp-MQMAS acquisition of I = 5/2 nuclei and also on a possible use of {^{27}Al}-^{1}H WURST-coslp-MQ-HETCOR experiments at ν_R = 62.5 kHz. We then extend our analysis to a higher spin value, using ^{93}Nb (I = 9/2) in $Cs_4Nb_{11}O_{30}$ ($C_Q \approx$ 15 MHz).[35,41] In the final section, we account for the differences of coslp-MQ behaviors between I = 3/2 and 5/2 spin systems, using numerical simulations with ^{23}Na and ^{27}Al nuclei.

II. Methods

All experiments were performed using a Bruker Avance NEO spectrometer with a B_0 = 14.1 T wide-bore magnet at a Larmor frequency of ν_0 = 58 (^{85}Rb), 156.4 (^{27}Al) and 146.9 (^{93}Nb) MHz, equipped with HX MAS probes using either ∅ = 3.2 mm rotors at ν_R = 16 or 21 kHz or ∅ = 1.3 mm at ν_R = 62.5 kHz. The spinning stability was maintained by a MAS III unit within ±10 Hz. Maximum RF fields of ν_1 = 43 (^{85}Rb) and 61 (^{27}Al) kHz were attained with ∅ = 3.2 mm, and ν_1 = 130 (^{27}Al) and 100 (^{93}Nb) kHz with ∅ = 1.3 mm. All powder samples were packed as purchased or as synthesized.

The MQMAS/STMAS pulse sequences for I > 3/2 spin systems used in this study are summarized in Figs.**1** and **S1**, for split-t_1 shifted-echo (or full-echo) and z-filter acquisitions, respectively, and in Fig.**S2** for {I}-^{1}H MQ/ST-HETCOR experiments. It must be noted that even if the number and type (hp, lp, coslp or CT-selective) of rf-pulses in the sequences do not depend on the spin value, the timings and selected coherence levels used in the pulse programs are different between those used with I = 3/2,[31] or I > 3/2 (here). Examples of TopSpin pulse programs for WURST-coslp-MQMAS and WURST-coslp-MQ-HETCOR experiments are provided in the SI of this article for I > 3/2 and in that of our previous study for I = 3/2.[31] Prior to any STMAS acquisition, an accurate adjustment of the spinning axis to the magic angle was performed using a DQF version of the split-t_1 shifted-echo pulse sequence on the sample of interest itself.[42] Chemical shift scales, shown in ppm, were referenced using the sample of interest itself as a secondary reference, and all 2D spectra were referenced according to the unified representation.[43]

All simulations were performed using the SIMPSON program.[44] The quadrupolar interaction up to the second-order was taken into account with η_Q = 0, without scalar or dipolar coupling. The input variables were, the nucleus of interest, the spinning frequency (ν_R), the RF amplitude (ν_1) and offset (ν_{off}), and the quadrupolar coupling constant (C_Q). To calculate the transfer efficiency, coherences were chosen to emulate the pulse sequences without any delay, except for the rotor-synchronized STMAS experiments (t_{1min} = τ_R - p1/2 – p4 - p2/2).

In high-resolution methods, the efficiency is defined as the ratio between the MQMAS or STMAS CT final signal and that observed after a CT-selective 90° pulse. The powder averaging parameters (i.e. crystal file and number of γ-angles) and the maximum time step Δt over which the Hamiltonian is considered time-dependent were tested for convergence, and a combination of ZCW54,[45–47] with 10 γ-angles and Δt = 0.1 μs was sufficient for the given range of C_Q values used in the plots. Since both the real (Re) and imaginary (Im) parts of the signal were found to be significant, its magnitude ($\sqrt{(Re^2 + Im^2)}$) is plotted as the signal intensity, unless stated otherwise. Further simulation details are given in the figure captions.

III. Results and discussion

We first briefly remind of a few essential practical points behind these WURST-lp/coslp-MQ-based experiments established in the previous studies of I = 3/2 spin systems.[25–27,31] (i) For MQ excitation/conversion, the two τ_R-pulses need to be identical and symmetrically applied to produce a coherent evolution of the two inner STs,[25,26] to serve as inversion pulses between the ±1Q-CT and ±3Q coherences. (ii) In lp-MQMAS, the τ_R-pulses are applied far off-resonance from the CT signals with a large offset (ν_{irr}) on the ST manifold,[25] whereas in coslp-MQMAS, the τ_R-pulses are applied near to the CT signals (ν_{irr}), ideally on the center-band

position of the inner STs, and are cosine-modulated (ν_{cos}).[26] (iii) The optimum RF field of the τ_R-pulses depends on the spinning frequency and the spin and C_Q values, and its amplitude in coslp-MQMAS,

$$\nu_{1,opt} \approx [C_Q\nu_R/(2I(2I-1))]^{1/2}, \quad (1)$$

is approximately $\sqrt{2}$ higher compared to lp-MQMAS.[26,31] In the following paragraphs, these technically essential points are similarly illustrated using I = 5/2 spin systems.

III.1. ^{85}Rb NMR of $RbNO_3$ (C_Q = 3.3-4.2 MHz) and Rb_2SO_4 (C_Q = 5 & 11 MHz) at ν_R = 21 kHz

^{85}Rb is a I = 3/2 low-gamma nucleus ($\nu_0 \approx$ 58 MHz at 14.1 T) with a natural abundance of 72.2 % and along with the ^{87}Rb other isotope (I = 5/2), ^{85}Rb has been employed in ssNMR method development owing to its favourable relaxation properties (e.g. $T_1 \approx$ a few hundred ms).[36] The sensitivity-limiting factor in conventional MQMAS/STMAS signal acquisition of such low-gamma nuclei is the small maximum RF field attainable for the hard-pulses by the conventional ssNMR setup. Here, using $^{85}RbNO_3$ and $^{85}Rb_2SO_4$, we demonstrate the sensitivity advantage of WURST-coslp-MQMAS acquisition for low-gamma nuclei within the maximum RF field achievable (43 kHz) by our 3.2 mm MAS probes. Three ^{85}Rb species exist in $RbNO_3$ and two in Rb_2SO_4, with (δ_{cs} (ppm), C_Q (MHz), η_Q) = (-27.4, 3.3, 0.2), (-28.9, 4.2, 0.9), (-31.6, 3.4, 0.6) and (42, 5, 0.9), (16, 11.0, 0.1).[34,35]

Fig.**2** shows a comparison of the isotropic projections of 2D ^{85}Rb DQF-STMAS and hp-, WURST-lp-, WURST-coslp-MQMAS spectra of $RbNO_3$ and Rb_2SO_4 with z-filter and full-echo acquisition. We observe that the WURST-coslp-MQMAS sensitivity is 3-4 times higher than the conventional hp-MQMAS and as good as the STMAS equivalent, especially with full-echo acquisition. Moreover, the best resolution is always observed with WURST-coslp-MQMAS, as best seen for the two close resonances of $RbNO_3$. For crystalline compounds, the full-echo acquisition shows a sensitivity advantage over the z-filter equivalent, especially for samples with large C_Q values and/or small losses (few or no ^{1}H nuclei).[48] Thanks to these advantages of sensitivity and resolution, WURST-coslp-MQMAS allows with full-echo acquisition the observation in Rb_2SO_4 of the species with C_Q = 11 MHz at ca. -140 ppm. This was impossible with all other sequences. It should be emphasized that the WURST sensitivity enhancement gives rise to a factor of 2.5-3.0 increase in the lp/coslp-MQMAS intensity (not shown). This is verified via numerical simulations (Fig.**S3**), which summarize at ν_R = 21 kHz the simulated ^{85}Rb WURST signal gain for $RbNO_3$ and Rb_2SO_4, with respect to the WURST RF field ($\nu_{1,WURST}$) and offset frequency (ν_{off}). It can be seen that WURST is robust with respect to RF field and offset, given the range of $\nu_{1,WURST}$ = 10-20 kHz and ν_{off} > 200 kHz. It must be noted that on the contrary, WURST sweeps do not bring any signal enhancement with hp-MQMAS.

Similarly, Fig.**3** shows the simulated ^{85}Rb signal intensity profiles of the same four MQMAS/STMAS sequences with respect to C_Q and ν_1 RF-field of the MQ/ST excitation/conversion pulses. In consistence with the experimental results, the conventional hp-MQMAS is globally inefficient within the practically attainable ^{85}Rb RF range limited to ν_1 < 43 kHz for ∅ = 3.2 mm, whereas WURST-coslp-MQMAS performs even better than the DQF-STMAS counterpart, owing to the intrinsically low RF requirement of the τ_R-pulses.

Here, it is worth reminding that, upon setting up the τ_R-pulses of the coslp-MQMAS experiment, the RF field (ν_1) and the cosine modulation (ν_{cos}) and carrier (ν_{irr}) frequencies need being optimized on the sample, especially with large C_Q values.[26,31]

The first two of these points are illustrated in Fig.**S4**, using the experimental ^{85}Rb WURST-coslp-MQMAS signal intensity profiles of $RbNO_3$ and Rb_2SO_4. For these two compounds, ν_{cos} = 100-200 kHz was found to be optimum and, since C_Q is larger in Rb_2SO_4 (C_Q = 5 and 11 MHz) than $RbNO_3$ (C_Q = 3.3-4.2 MHz), the optimum RF is larger in Rb_2SO_4 ($\nu_1 \approx$ 30 kHz) than $RbNO_3$ ($\nu_1 \approx$ 20 kHz) (see Eq.1). For the third point, the offset positioning is more adverse in Rb_2SO_4 than $RbNO_3$ because the inner ST center-band lies far away from the CT for large C_Q sites. This is illustrated in Fig.**S5**, by a comparison of experimental ^{85}Rb WURST-coslp-MQMAS signal intensity profiles of $RbNO_3$ and Rb_2SO_4, with respect to the irradiation frequency (ν_{irr}). In $RbNO_3$, changing the offset position of τ_R-pulses by ±8 kHz results in no apparent change in intensity, whereas in Rb_2SO_4, $\nu_{irr} \approx$ 8 kHz needs to be applied for the best sensitivity.

Overall, our experiments and numerical simulations have verified that the WURST-coslp-MQMAS sensitivity is 3-4 times higher than the conventional hp-MQMAS for ^{85}Rb, and even better than the STMAS equivalent without the precise adjustment of spinning axis to the magic angle. Hence, WURST-coslp-MQMAS is highly recommended for low-gamma nuclei, for which the large RF requirement of conventional hp-MQMAS cannot be satisfied and/or with large C_Q samples for which the MQ excitation/conversion efficiency is expected to be intrinsically low.

III.2. ^{27}Al NMR of $AlPO_4$-Berlinite (C_Q = 4.0 MHz) at ν_R = 16 kHz

Having demonstrated the sensitivity advantage of WURST-coslp-MQMAS with the low-gamma ^{85}Rb isotope, we envisaged to extend the use of cosine-modulation to moderate-gamma nuclei, ^{27}Al, aiming to extrapolate the results to {^{27}Al}-^{1}H MQ-HETCOR experiments under fast MAS conditions.

First, we employed a single ^{27}Al site compound, $AlPO_4$-Berlinite (C_Q = 4.0 MHz),[35,37] at ν_R = 16 kHz to check the ^{27}Al WURST-coslp-MQMAS sensitivity in comparison with other conventional methods. The isotropic projections of 2D ^{27}Al DQF-STMAS and hp-, WURST-lp-, WURST-coslp-MQMAS spectra of $AlPO_4$-berlinite are summarized, with z-filter and full-echo acquisitions, in Fig.**S6**.

As often verified for samples with small-moderate C_Q values, the full-echo approach is here less favourable than the z-filter counterpart, due to the required long echo delay (τ_{echo} = 5 ms). With this high Larmor frequency (156.4 MHz), a sufficiently high RF-field (ν_1 = 61 kHz) is achievable with ∅ = 3.2 mm rotors, and hence STMAS is best for sensitivity, on condition that the spinning axis is accurately set to the magic angle prior to the signal acquisition. However, although not as good as STMAS, the WURST-coslp-MQMAS sensitivity was found better than the conventional hp-MQMAS, with a very much reduced RF requirement ($\nu_1 \approx 18$ instead of 61 kHz).

III.3. ^{27}Al NMR of Al(acac)$_3$ + Al(lact)$_3$ (C_Q = 3, 5 MHz) at ν_R = 16 kHz

We then chose a 1:1 molar mixture of Al(acac)$_3$ + Al(lact)$_3$, each containing one single ^{27}Al site, with C_Q = 3.0 and 5.0 MHz, respectively.[15,38] By observing the ^{27}Al isotropic resonances, we reckon that Al(acac)$_3$ exhibits a crystalline nature with a sharp, well-defined peak, while Al(lact)$_3$ has a more distributed character with a broad, featureless peak. This is reflected in Fig.**4**, which shows the isotropic projections of this mixture recorded with 2D ^{27}Al DQF-STMAS and hp-, WURST-lp-, WURST-coslp-MQMAS sequences at ν_R = 16 kHz, with z-filter and full-echo acquisitions.

These spectra are fully in agreement with those observed with AlPO$_4$-Berlinite: (i) the z-filter acquisition is better than full-echo for these protonated samples with moderate C_Qs, (ii) DQF-STMAS shows the highest sensitivity, but with ν_1 = 61 kHz and a perfectly adjusted magic-angle, and (iii) for Al(acac)$_3$ WURST-coslp-MQMAS with only ν_1 = 15 kHz is better than the conventional hp-MQMAS with 61 kHz. For Al(lact)$_3$, the WURST-coslp-MQMAS sensitivity gain is slightly smaller due to the distribution of surrounding.

III.4. ^{27}Al NMR of ipa-AlPO$_4$-14 (C_Q = 1.8-5.4 MHz) at ν_R = 62.5 kHz

Aiming for {^{27}Al}-^{1}H WURST-coslp-MQ-HETCOR detection, we then switched to a small rotor diameter, ∅ = 1.3 mm, and performed the equivalent set of experiments with ν_R = 62.5 kHz, using ipa-AlPO$_4$-14. This compound contains four ^{27}Al sites showing isotropic peaks from left to right: (δ_{cs} (ppm), C_Q (MHz), η_Q) = (42.2, 1.8, 0.6), (45.0, 4.1, 0.8), (27.0, 5.4, 0.9), (-0.2, 2.6, 0.9). It has been known that the STMAS signals of ipa-AlPO$_4$-14 are motionally broadened due to the presence of μs dynamics around Al nuclei,[5] which makes high-resolution MQMAS and STMAS acquisitions complementary to each other. For coslp-MQMAS, it is worth remembering that the optimum RF-field of the τ_R-pulses depends not only on the C_Q value, but also on the spinning frequency (Eq.1).[26,31] This is verified in our ^{27}Al experimental observations, shown in Figs.**4**, **5**, and **S6**, where the optimum RF-field of the τ_R-pulses increased from $\nu_1 \approx 18$ to 30-66 kHz, as the spinning frequency increased from ν_R = 16 to 62.5 kHz.

Upon WURST-coslp-MQMAS acquisition of ipa-AlPO$_4$-14, we observed two additional complexities.

First, for such samples containing multiple ^{27}Al sites with a wide range of C_Q values, the coslp-MQMAS variables need to be chosen as a compromise over the optimum ranges for all sites, which consequently led to only a marginal increase in the sensitivity overall. As a result, the signal intensities observed with WURST coslp-MQMAS are smaller than with DQF-STMAS, and they are similar to those recorded with hp-MQMAS (Fig.**5**). However, the required RF-field was much smaller with WURST-coslp-MQMAS (30 or 66 kHz) than with DQF-STMAS and hp-MQMAS (121 kHz), and no stringent magic angle set up was required.

Second, when phasing a 2D full-echo hp-MQMAS spectrum, one can usually use the same phase correction parameters as for the analogous 1D spectrum from which the 2D dataset is created. However, when phasing the 2D full-echo WURST-coslp-MQMAS spectra, we needed to perform the 2D phase correction from scratch (i.e. discarding the phase parameters from the 1D dataset) to find the parameters that simultaneously produce a properly-phased 2D spectrum along the MAS and isotropic dimensions. We suspect that this 2D phasing complexity originates from the phase evolution during the τ_R-pulses. This phase issue did not arise in AlPO$_4$-berlinite with a single Al site or Al(acac)$_3$ + Al(lact)$_3$ with close C_Q values, but was noticeable with ipa-AlPO$_4$-14 containing multiple ^{27}Al sites with a wide range of C_Q values. Based on our hands-on experience, we suggest the following step-by-step phasing protocol when encountering such phasing issues upon full-echo acquisition: 1) reset all phases. 2) Calculate an approximate first-order correction in F2, such as 180*(τ_{echo} + 3τ_R)/(dwell-time). Here, the additional evolution on 3Q during the long τ_R pulses must be considered. 3) Do the 2D Fourier transform. 4) Phase the F1 dimension to have two neighbouring peaks well phased. 5) Correct the first-order term in F2 by a small amount. 6) Repeat steps 3 to 5 until all peaks are well phased. It must be noted that this way of phasing is very close to that described previously for 2D lp-MQMAS spectra.[25]

Fortunately, this phase issue is less critical in the 2D {^{27}Al}-^{1}H MQ/ST-HETCOR spectra, because the signals are narrow along the two dimensions with high spinning speeds. Fig.**6** compares the 1D {^{27}Al}-^{1}H MQ/ST-HETCOR ^{1}H spectra of ipa-AlPO$_4$-14 at ν_R = 62.5 kHz, recorded with ST and ST-SPAM,[15] hp-MQ and hp-MQ-SPAM,[14,15] WURST-lp-MQ and WURST-coslp-MQ approaches. The SPAM (Soft-Pulse Added-Mixing) scheme has been used here, because it increases the efficiency of the second hard-pulse and only differs from the conventional hp-MQMAS and STMAS approaches by a change in the phases.[48–50] Due to the fact that the coslp-MQ variables result from a compromise over the wide C_Q range, we observed no sensitivity advantage in {^{27}Al}-^{1}H WURST-coslp-MQ-HETCOR acquisition of ipa-AlPO$_4$-14. It should be remembered that, as in STMAS and STMAS-SPAM, the isotropic dimension of ST-HETCOR spectra of ipa-AlPO$_4$-14 (Fig. 5) is broadened by μs dynamics around Al nuclei,[5] and thus the required accuracy of magic angle setting is then not as stringent as expected for other crystalline samples. Therefore, in this particular case, we

recommend the use of the two MQ/ST-SPAM-HETCOR acquisitions, for the ease of setup and the best sensitivity, in spite of the higher RF-field than with WURST-coslp-MQ-HETCOR (121 v.s. 54 kHz),

To summarize, for high-gamma nuclei (e.g. ^{27}Al) with moderately large C_Q values (e.g. > 4 MHz), ^{27}Al WURST-coslp-MQMAS can perform slightly better than the conventional hp-MQMAS, but with a much reduced RF requirement. For {^{27}Al}-^{1}H MQ-HETCOR under fast MAS, MQ/ST-SPAM-HETCORs may be the methods of choice for the ease of setup, especially when multiple sites with a large variety of C_Q values are present.

III.5. ^{93}Nb (I = 9/2) NMR of $Cs_4Nb_{11}O_{30}$ (C_Q = 15 MHz) at ν_R = 62.5 kHz

In a last step, we have extended the τ_R-pulses high-resolution methods to higher spin-value nuclei, and we have chosen ^{93}Nb (I = 9/2) of $Cs_4Nb_{11}O_{30}$, which contains a single species with $C_Q \approx 15$ MHz and $\eta_Q \approx 0.6$.[35,41] We have used a fast spinning speed of ν_R = 62.5 kHz, to minimize the numerous spinning sidebands of this broad second-order MAS spectrum. In Fig.**7**, we show the isotropic projections of the ^{93}Nb 2D DQF-STMAS and hp-, WURST-lp-, WURST-coslp-MQMAS spectra, with z-filter and full-echo acquisitions. The best sensitivity is observed with DQF-STMAS, but this experiment requires a perfect setting of the magic angle, a very stable spinning speed and a high RF-field (ν_1 = 100 kHz). The second best sensitivity is observed with WURST-coslp-MQMAS, especially with the z-filter acquisition. This robust method is more efficient than the hp-MQMAS sequence and only requires a small RF-field of 14 kHz, instead of 100 kHz for the hp-MQMAS version.

III.6. Comparison between ^{23}Na (I = 3/2) and ^{27}Al (I = 5/2) WURST-coslp-MQMAS at ν_R = 20 kHz

In the previous sections, we have demonstrated that for nuclei with spin value higher than 3/2, WURST-coslp-MQMAS always requires a small RF-field and is hence simultaneously favorable from the sensitivity point of view in the cases of (i) low-gamma nuclei, (ii) large rotor diameters used for insensitive nuclei, and (iii) large C_Q sites. However, its sensitivity is less well performing with MQMAS and MQ-HETCOR acquisitions of high-gamma nuclei. Here, we remind of our previous I = 3/2 investigations,[31] which revealed a general large sensitivity advantage of WURST-coslp-MQMAS based acquisitions, not only for low-gamma isotopes (e.g. ^{35}Cl) or large C_Q sites (e.g. ^{71}Ga), but also for high-gamma ^{87}Rb and ^{23}Na MQMAS and MQ-HETCOR experiments. In this last section, we briefly account for the difference in WURST-coslp-MQMAS behaviors between I = 3/2 and 5/2 spin systems, using numerical simulations of ^{23}Na and ^{27}Al nuclei. We chose this pair of nuclei as their Larmor frequencies are close to each other (158.7 and 156.4 MHz at 14.1 T, respectively).

In Fig.**S7** we show the simulated ^{23}Na and ^{27}Al WURST gains at ν_R = 20 kHz, with respect to the WURST RF amplitude ($\nu_{1,WURST}$) and offset (ν_{off}). We used C_Q values of 2 and 6.6 MHz for ^{23}Na and ^{27}Al, respectively, to account for the factor defining the quadrupolar interaction with respect to $\nu_Q = 3C_Q/(2I(2I-1))$. We observe that the combination of WURST with ν_{off} = 300 and ν_1 = 20 kHz can be safely employed for both nuclei. We also note that the WURST gain increases from ca. 2.0 to 2.7 when going from a spin-3/2 to a spin-5/2 nucleus. This rise is related to the increased number of STs; the higher the spin value the larger the WURST gain.

In Fig.**8**, we summarize the simulated ^{23}Na (I = 3/2) and ^{27}Al (I = 5/2) signal intensities of hp-MQMAS and WURST-coslp-MQMAS at ν_R = 20 kHz, with respect to C_Q and the RF-field (ν_1) of the excitation/conversion pulses.

First, upon comparison of the conventional hp-MQMAS results, one may note that I = 5/2 requires a lower minimum RF-field than I = 3/2, ca. 40 instead of 70 kHz, for a relatively effective 3Q excitation/conversion. This point partly contributes to the favorable comparison of the WURST-coslp-MQMAS performance of 3/2 spin over the 5/2 equivalent, as the sensitivity is generally compared with respect to the conventional hp-MQMAS.

Second, the overall WURST-coslp-MQMAS efficiency is globally twice higher for I = 3/2 than for 5/2. The efficiency of the coslp-MQMAS transfer is related to the coherent inversions of the two inner STs by the τ_R-pulses, such that the initial 3Q coherences created by the first τ_R-pulse are refocused by the second one.[25,26] For I = 3/2 spin systems, only these inner STs exist, and thus the coherences are well-confined, and this refocusing is consequently highly efficient. The signal is observable with an RF-field of ca. 20 kHz, and is maximum at about 70 kHz, with intensities of ca. 0.6 and 0.9, respectively (Fig.**8b**). For I > 3/2 nuclei, on the contrary, due to the presence of other STs, a coherence leakage to these STs is inevitably observed during the selective inversion of the inner-most STs. The signal starts with an RF-field of ca. 10 kHz, and is maximum with an intensity of ca. 0.5 at about 20 kHz. For higher RF-fields, the leakage process largely decreases the sensitivity (Fig.**8d**).

IV. Conclusions

Following the recent development of WURST-coslp-MQMAS, which enables an efficient MQ excitation/conversion of I = 3/2 nuclei with a reduced RF-field, we extend our previous discussions to higher spin values in the context of high-resolution MQMAS and MQ-HETCOR experiments.

As general rules, we have shown that for all spin values the WURST CT enhancement is effective leading to a signal gain of ca. 2-3, and that the WURST-coslp-MQMAS acquisition (i) does not have to be rotor-synchronized, contrary to STMAS, to expand the spectral width, as example when using large rotor diameters, (ii) requires a small RF-amplitude, contrary to STMAS and hp-MQMAS methods, and (iii) enhances the resolution with respect to other conventional methods.

The sensitivity advantage for spin-5/2 nuclei of WURST-coslp-MQMAS acquisition has been experimentally demonstrated for low-gamma nuclei and/or large C_Q values using $^{85}RbNO_3$ and $^{85}Rb_2SO_4$.
For high-gamma nuclei with spin larger than 3/2 (e.g. ^{27}Al) and with moderate C_Q values, the use of WURST-coslp-MQMAS and {I}-^1H WURST-coslp-MQ-HETCOR experiments under fast MAS conditions has been demonstrated. However, the sensitivity advantage related to the two $\pm$1Q-CT $\leftrightarrow$ $\pm$3Q coslp transfers is then largely decreased, especially in the case of samples with very different C_Q values, and other approaches based on composite pulses, eg. hp + SPAM, are more efficient.

The WURST-coslp-MQMAS high resolution method has been demonstrated with higher spin values, i.e. I = 9/2 with ^{93}Nb isotope, and the method has also shown a small RF requirement.

The difference in WURST-coslp-MQ behaviors between I = 3/2 and I $\geq$ 5/2 spins has been elucidated using simulations on ^{23}Na and ^{27}Al nuclei. For I = 3/2 spin systems, only inner STs exist and the transfer of coherences is well-confined and hence efficient. For I $\geq$ 5/2 nuclei, on the contrary, due to the presence of other STs, a coherence leakage to these extra STs occurs during the selective inversion of the inner-most STs, and the efficiency is decreased.
Nevertheless, the sensitivity advantage of this method, which uses weak RF-fields, offers a great promise for (i) low-gamma nuclei, (ii) large rotor diameter rotors used with insensitive nuclei, or (iii) samples with large C_Q values; for which conventional approaches fail to produce sufficient MQ signals with hard-pulses. We predict that WURST-coslp-MQMAS will expand the range of nuclei and C_Q values that can be further investigated using high-resolution quadrupolar NMR.

Conflicts of interest

There are no conflicts to declare.

Acknowledgements

H.N. acknowledges JSPS Grant-in-Aid for Early-Career Scientists (JP20K15319) and JST, PRESTO Grant Number JPMJPR2276. Authors thank Z. Gan and I. Hung for their fruitful scientific discussions.

References

1 E.R. Andrew, A. Bradbury, R.G. Eades, *Nature*, **1958**, 182, 1659.
2 L. Frydman, J.S. Harwood, *J. Am. Chem. Soc.*, **1995**, 117, 5367–5368.
3 Z. Gan, *J. Am. Chem. Soc.*, **2000**, 122, 3242–3243.
4 S.E. Ashbrook, S. Antonijevic, A.J. Berry, S. Wimperis, *Chem. Phys. Lett.*, **2002**, 364, 634–642.
5 S. Antonijevic, S.E. Ashbrook, S. Biedasek, R.I. Walton, S. Wimperis, H. Yang, *J. Am. Chem. Soc.*, **2006**, 128, 8054–8062.
6 A. Goldbourt, E. Vinogradov, G. Goobes, S. Vega, *J. Magn. Reson.*, **2004**, 169, 342–350.
7 J. Trébosc, O. Lafon, B. Hu, J.-P. Amoureux, *Chem. Phys. Lett.*, **2010, 496**, 201–207.
8 N. Merle, J. Trébosc, A. Baudouin, I. Del Rosal, L. Maron, K. Szeto, M. Genelot, A. Mortreux, M. Taoufik, L. Delevoye, R.M. Gauvin, *J. Am. Chem. Soc.*, **2012**, 134, 9263–9275.
9 B. Bouchevreau, C. Martineau, C. Mellot-Draznieks, A. Tuel, M.R. Suchomel, J. Trébosc, O. Lafon, J.-P. Amoureux, F. Taulelle, *Chem. Mater.*, **2013**, 25, 2227–2242.
10 J. Wack, R. Siegel, T. Ahnfeldt, N. Stock, L. Mafra, J. Senker, *J. Phys. Chem. C*, **2013**, 117, 19991–20001.
11 M.K. Pandey, H. Kato, Y. Ishii, Y. Nishiyama, *Phys. Chem. Chem. Phys.*, **2016**, 18, 6209–6216.
12 A. Venkatesh, M.P. Hanrahan, A.J. Rossini, *Solid State Nucl. Magn. Reson.*, **2017**, 84, 171–181.
13 N.T. Duong, Y. Nishiyama, *Solid State Nucl. Magn. Reson.*, **2017**, 84, 83–88.
14 A. Sasaki, J. Trébosc, J.-P. Amoureux, *J. Magn. Reson.*, **2021**, 329, 107028.
15 A. Sasaki, J. Trébosc, J.-P. Amoureux, *J. Magn. Reson.*, **2021**, 333, 107093.
16 J.-P. Amoureux, M. Pruski, D.P. Lang, C. Fernandez, *J. Magn. Reson.*, **1998**, 131, 170–175.
17 G. Wu, D. Rovnyak, R.G. Griffin, *J. Am. Chem. Soc.*, **1996**, 118, 9326–9332.
18 P.K. Madhu, A. Goldbourt, L. Frydman, S. Vega, *Chem. Phys. Lett.*, **1999**, 307, 41–47.
19 H. Colaux, D.M. Dawson, S.E. Ashbrook, *J. Phys. Chem. A*, **2014**, 118, 6018–6025.
20 A.P.M. Kentgens, R. Verhagen, *Chem. Phys. Lett.*, **1999**, 300, 435–443.
21 T. Vosegaard, P. Florian, D. Massiot, P.J. Grandinetti, *J. Chem. Phys.*, **2001**, 114, 4618–4624.
22 R. Siegel, T.T. Nakashima, R.E. Wasylishen, *Chem. Phys. Lett.*, **2005**, 403, 353–358.
23 Z. Yao, H.T. Kwak, D. Sakellariou, L. Emsley, P.J. Grandinetti, *Chem. Phys. Lett.*, **2000**, 327, 85–90.
24 T. Vosegaard, F.H. Larsen, H.J. Jakobsen, P.D. Ellis, N.C. Nielsen, *J. Am. Chem. Soc.*, **1997**, 119, 9055–9056.
25 I. Hung, Z. Gan, *J. Magn. Reson.*, **2021**, 324, 106913.

26 I. Hung, Z. Gan, *J. Magn. Reson.*, **2021**, 328, 106994.
27 I. Hung, Z. Gan, *Phys. Chem. Chem. Phys.*, **2020**, 22, 21119–21123
28 Ē. Kupče, R. Freeman, *J. Magn. Reson. Ser. A*, **1995**, 115, 273–276.
29 E. Kupče, R. Freeman, *J. Magn. Reson. Ser. A*, **1996**, 118, 299–303.
30 K.K. Dey, S. Prasad, J.T. Ash, M. Deschamps, P.-J. Grandinetti, *J. Magn. Reson.*, **2007**, 185, 326–330.
31 A. Sasaki, J. Trébosc, H. Nagashima, J.-P. Amoureux, *J. Magn. Reson.*, **2022**, 345, 107324.
32 I. Hung, E.G. Keeler, W. Mao, P.L. Gor, R.G. Griffin, Z. Gan, *J. Phys. Chem. Lett.*, **2022**, 13, 6549−6558.
33 I. Hung, W. Mao, E.G. Keeler, R.G. Griffin, P.L. Gor'kov, Z. Gan, *Chem. Commun.*, **2023**, 59, 3111-3113.
34 I. Hung, A. Wong, A.P. Howes, T. Anupõld, A. Samoson, M.E. Smith, D. Holland, S.P. Brown, R. Dupree, *J. Magn. Reson.*, **2009**, 197, 229–236.
35 A. Sasaki, Y. Tsutsumi, J.-P. Amoureux, *Solid State Nucl. Magn. Reson.*, **2020**, 108, 101668.
36 J.T. Cheng, J.C. Edwards, P.D. Ellis, *J. Phys. Chem.*, **1990**, 94, 553–561.
37 D. Massiot, F. Fayon, B. Alonso, J. Trébosc, J.-P. Amoureux, *J. Magn. Reson.*, **2003**, 164, 160–164.
38 S.E. Ashbrook, S. Wimperis, *Chem. Phys. Lett.*, **2001**, 340, 500–508.
39 C. Fernandez, J.-P. Amoureux, J.-M. Chezeau, L. Delmotte, H. Kessler, *Microporous Mater.*, **1996**, 6, 331–340.
40 J.-P. Amoureux, C. Fernandez, S. Steuernagel, *J. Magn. Reson. A*, **1996**, 123, 116–118.
41 A. Flambard, L. Montagne, L. Delevoye, S. Steuernagel, *Solid State Nucl. Magn. Reson.*, **2007**, 32, 34–43.
42 J. Trébosc, J.-P. Amoureux and Z. Gan, *Solid State Nucl. Magn. Reson.*, **2007**, 31, 1–9.
43 J.-P. Amoureux, C. Fernandez, *Solid State Nucl. Magn. Reson.*, **1998,** 10, 211-223; J.-P. Amoureux, C. Huguenard, F. Engelke, F. Taulelle, *Chem. Phys. Lett.*, **2002**, 356, 497–504**.**
44 M. Bak, J.T. Rasmussen, N.C. Nielsen, *J. Magn. Reson.*, **2000**, 147, 296–330.
45 S.K. Zaremba, *Ann. di Mat. Pura ed Appl.*, **1966**, 73, 293–317.
46 H. Conroy, *J. Chem. Phys.*, **1967**, 47, 5307.
47 V.B. Cheng, H.H. Suzukawa, M. Wolfsberg, *J. Chem. Phys.*, **1973**, 59, 3992–3999.
48 J.-P. Amoureux, L. Delevoye, S. Steuernagel, Z. Gan, S. Ganapathy, L. Montagne, *J. Magn. Reson.*, **2005**, 172, 268–278.
49 Z. Gan, H.T. Kwak, *J. Magn. Reson.*, **2004**, 168, 346–351.
50 J.-P. Amoureux, L. Delevoye, G. Fink, F. Taulelle, A. Flambard, L. Montagne, *J. Magn. Reson.*, **2005**, 175, 285–299.

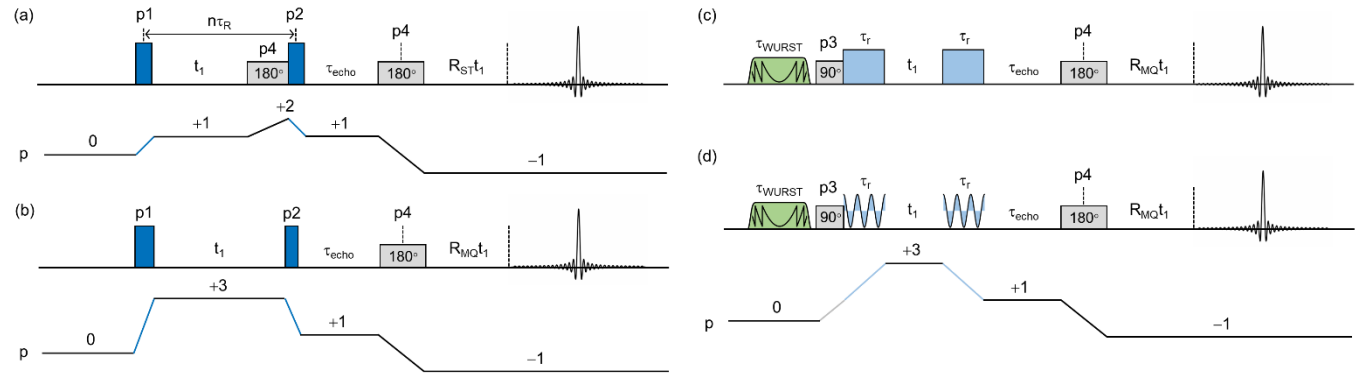

Fig.1. Pulse sequences and coherence transfer pathways for split-t_1 shifted-echo (or full-echo) acquisition: (a) DQF-STMAS, (b) hp-MQMAS, (c) WURST-lp-MQMAS and (d) WURST-coslp-MQMAS experiments, where $\{R_{MQ}, R_{ST}\} = \{19/12, 7/24\}$ for I = 5/2. It must be noted that MQMAS experiments shown in (b-d), can be performed unsynchronized ($t_1 \neq n\tau_R$) to increase the indirect spectral width.

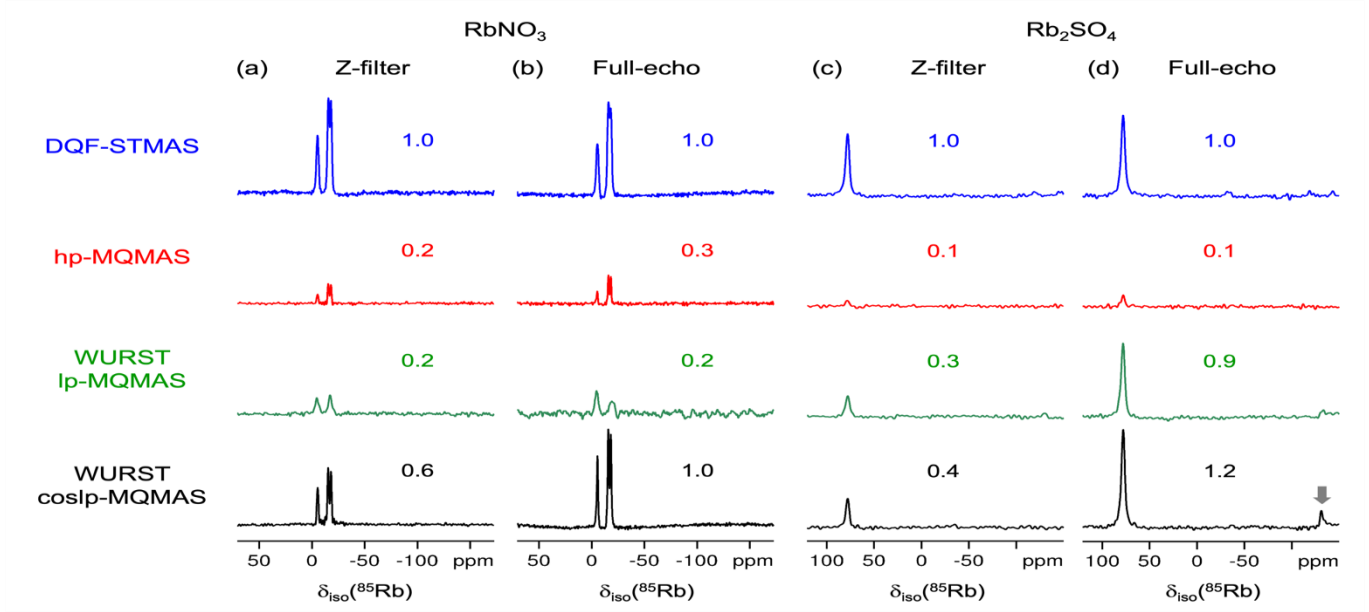

Fig.2. Comparison of the isotropic projections of 2D ^{85}Rb DQF-STMAS and hp-, WURST-lp-, WURST-coslp-MQMAS spectra of (a,b) $RbNO_3$ and (c,d) Rb_2SO_4 with RD = 0.25 s, and (a,c) z-filter (Z) or (b,d) full-echo (FE) acquisition (τ_{echo} = 4 ms), respectively. On each spectrum, the maximum intensity is indicated relative to that observed with DQF-STMAS. For the WURST coslp-MQMAS spectrum of Rb_2SO_4 acquired with full-echo, the second isotropic resonance at ca. -140 ppm is indicated with an arrow. **WURST**$_{80}$: τ_{WURST} = 1 ms, $\nu_{sweep} = \nu_R$ = 21, $\nu_{1,WURST}$ = 13, ν_{off} = +300 kHz.

DQF-STMAS and **hp-MQMAS**: the RF-field for the two hard-pulses was fixed at its maximum safe value (43 kHz) for the probe: ν_1 {p1, p2, p3, p4} = {43, 43, 10, 10} kHz.

<u>$RbNO_3$</u>: $T_{exp} \approx 0.8$ h each. NS {MQ/ST} = {24/32 (Z), 48/64 (FE)}, Δ_{t1} {MQ/ST} = {50/100} µs, N_{t1} = {384 (Z), 192 (FE)}.

WURST-lp-MQMAS: ν_1 {Z, FE} = {23, 19}, ν_{irr} {Z, FE} = {+350, +400} kHz. **WURST-coslp-MQMAS**: ν_1 {Z, FE} = {19, 19}, ν_{irr} = 0, ν_{cos} = 150 kHz.

<u>Rb_2SO_4</u>: T_{exp} = 2.0 h each. NS {MQ/ST} = {192/192 (Z), 384/384 (FE)}, Δ_{t1} {MQ/ST} = {45/90} µs, N_{t1} = {150 (Z), 75 (FE)}.

WURST-lp-MQMAS: ν_1 {Z, FE} = {30, 23}, ν_{irr} {Z, FE} = {+400, +300} kHz. **WURST-coslp-MQMAS**: ν_1 {Z, FE} = {30, 30}, ν_{irr} = 6, ν_{cos} = 150 kHz.

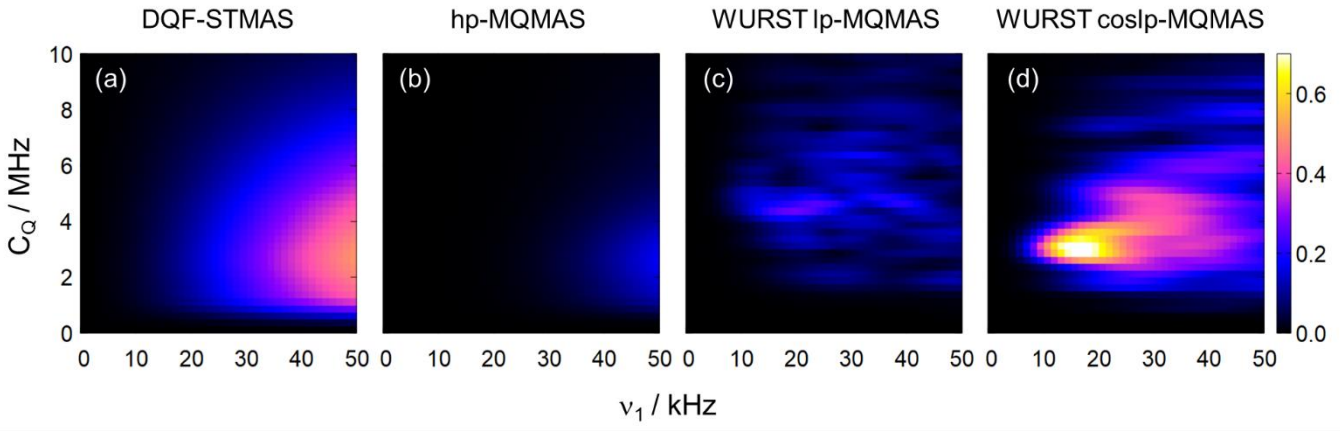

Fig.3. Simulated ^{85}Rb signal intensity of DQF-STMAS and hp-, WURST-lp-, WURST-coslp-MQMAS, with respect to C_Q and RF-field (ν_1) of the MQ/ST excitation and conversion pulses.

DQF-STMAS/hp-MQMAS: ν_1 (p3 & p4) = 10 kHz, {p1, p2, p3, p4} = {1.8, 1.2, 8, 16}/{4.0, 1.8, 8, 16} μs.

WURST-lp-MQMAS: ν_{irr} = +340 kHz. **WURST-coslp-MQMAS**: ν_{cos} = 200 kHz. **WURST$_{80}$**: τ_{WURST} = 1 ms, $\nu_{sweep} = \nu_R$ = 21, $\nu_{1,WURST}$ = 15, ν_{off} = +300 kHz.

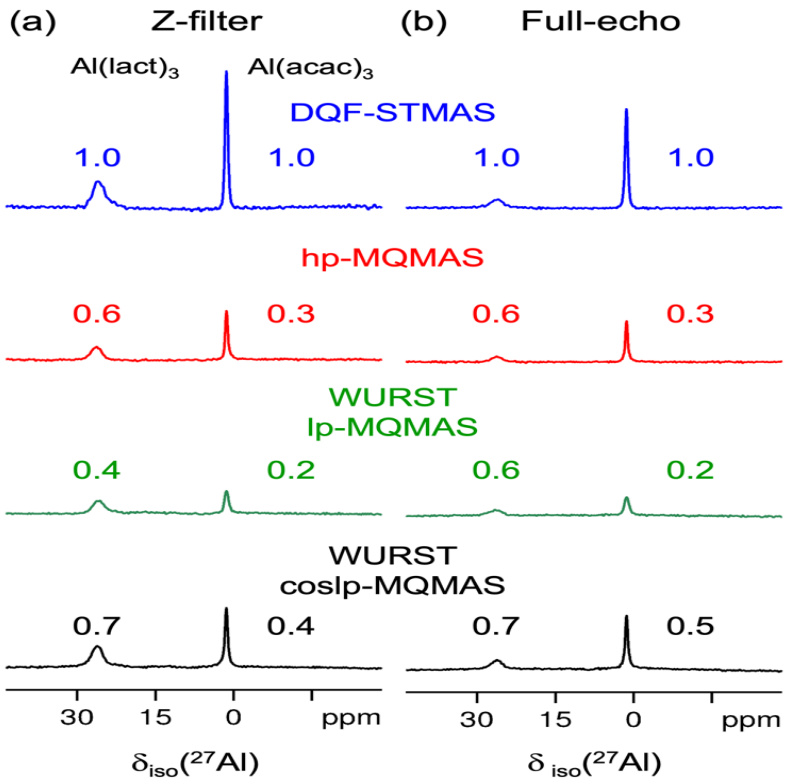

Fig.4. Al(acac)$_3$ + Al(lact)$_3$: comparison of isotropic projections of 2D ^{27}Al DQF-STMAS and hp-, WURST-lp-, WURST- coslp-MQMAS spectra with (a) z-filter and (b) full-echo (τ_{echo} = 10 ms) acquisitions. RD = 0.5 s, T_{exp} = 1.3-2.0 h each. On each spectrum the intensities are given relative to those with DQF-STMAS.

hp-MQMAS/DQF-STMAS: NS = {48/32 (Z), 96/64 (FE)}, Δ_{t1} = {62.5/125} μs, N_{t1} = {300 (Z), 150 (FE)}, ν_1 {p1, p2, p3, p4} = {61, 61, 5, 5} kHz.

WURST-lp-MQMAS: ν_1 {Z, FE} = 15, ν_{irr} {Z, FE} = {+150, +200} kHz. **WURST-coslp-MQMAS**: ν_1 = 18, ν_{irr} = 0, ν_{cos} = 200 kHz.

WURST$_{80}$: τ_{WURST} = 1 ms, $\nu_{sweep} = \nu_R$ = 16, $\nu_{1,WURST}$ = 10, ν_{off} = +250 kHz.

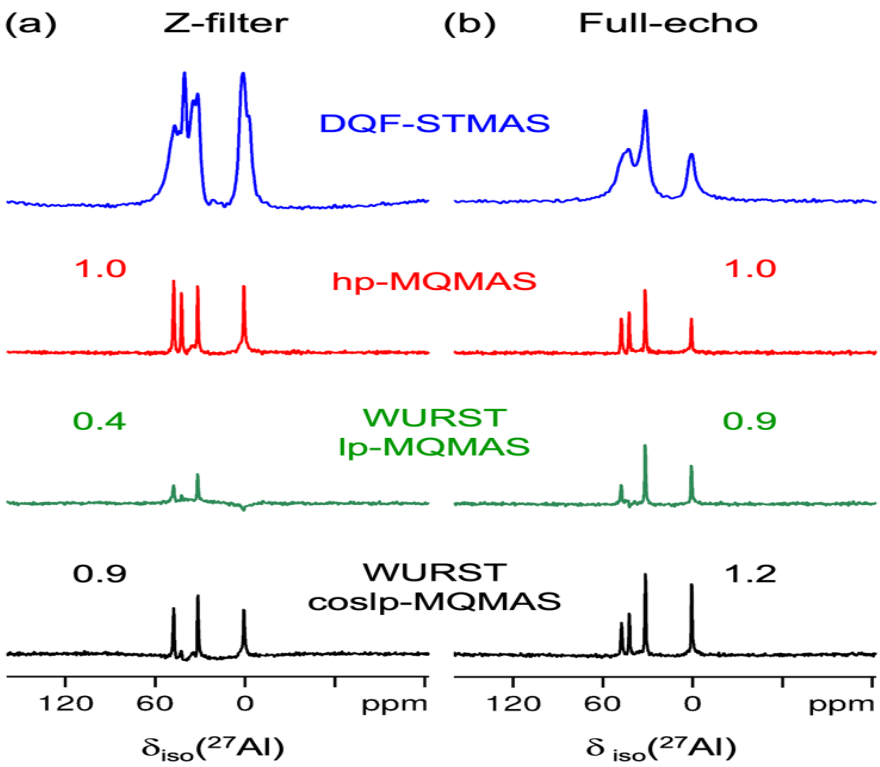

Fig.5. ipa-$AlPO_4$-14: comparison of isotropic projections of 2D ^{27}Al DQF-STMAS and hp-, WURST-lp-, WURST-coslp-MQMAS spectra with (a) z-filter and (b) full-echo (τ_{echo} = 6 ms) acquisitions. RD = 0.25 s, T_{exp} = 3.0 h each. On each spectrum, the intensity at $\delta_{iso} \approx 35$ ppm is indicated relative to that observed with hp-MQMAS. The DQF-STMAS spectra are not included in the comparison due to the motional broadening.

hp-MQMAS/DQF-STMAS: NS = {72/192 (Z), 144/384 (FE)}, Δ_{t1} = {16/32} μs, N_{t1} = {600/200 (Z), 300/100 (FE)}, ν_1 {p1, p2, p3, p4} = {121, 121, 10, 10} kHz.

WURST-lp-MQMAS: ν_1 {Z, FE} = {45, 30}, ν_{irr} {Z, FE} = {+400, +300} kHz. **WURST-coslp-MQMAS**: ν_1 {Z, FE} = {66, 30}, ν_{irr} = 0, ν_{cos} {Z, FE} = {400, 250} kHz. **WURST$_{80}$**: τ_{WURST} = 1 ms, $\nu_{sweep} = \nu_R$ = 62.5, $\nu_{1,WURST}$ = 13, ν_{off} = +250 kHz.

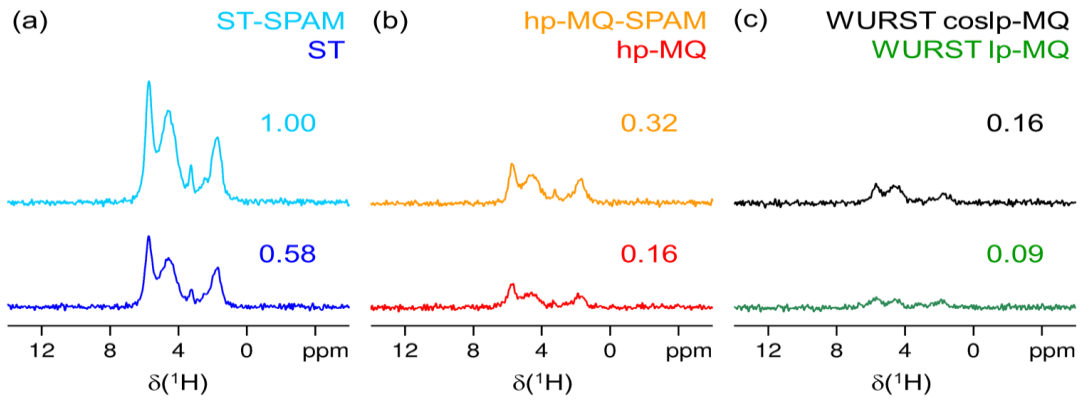

Fig.6. ipa-$AlPO_4$-14: comparison of 1D {^{27}Al}-^{1}H MQ/ST-HETCOR spectra with (a) ST and ST-SPAM, (b) hp-MQ and hp-MQ-SPAM, (c) WURST-lp-MQ and WURST-coslp-MQ approaches. NS = 96, RD = 0.5 s, T_{exp} = 48 s each. On each spectrum the maximum intensities are given relative to that with ST-SPAM.

MQ, MQ-SPAM, ST, ST-SPAM: ν_1 {p1, p2, p3, p4} = {121, 121, 10, 10} kHz. **WURST-lp-MQ**: ν_1 = 54, ν_{irr} = +400 kHz. **WURST-coslp-MQ**: ν_1 = 54, ν_{irr} = 0, ν_{cos} = 400 kHz. **WURST$_{80}$**: τ_{WURST} = 1 ms, $\nu_R = \nu_{sweep}$ = 62.5, $\nu_{1,WURST}$ = 13, ν_{off} = +250 kHz.

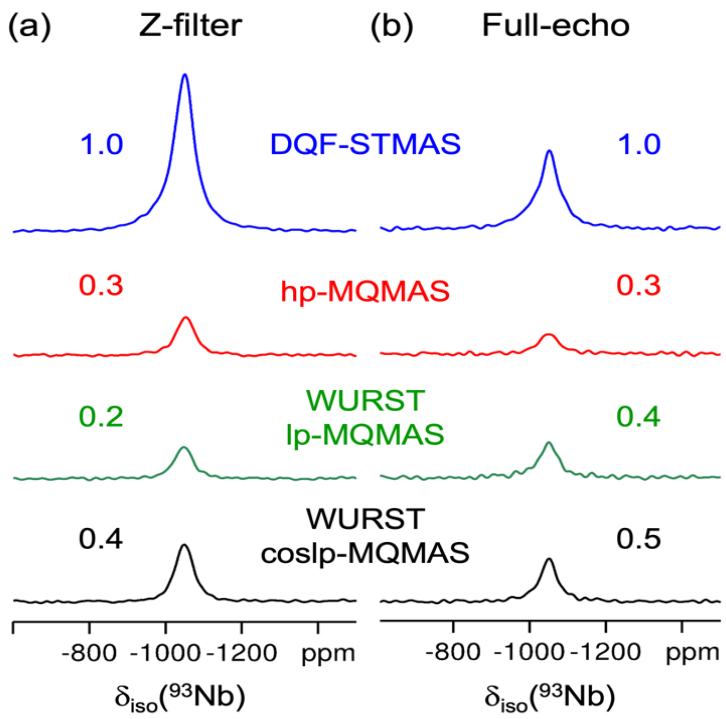

Fig.7. $Cs_4Nb_{11}O_{30}$. Comparison of isotropic projections of 2D ^{93}Nb DQF-STMAS and hp-, WURST-lp-, WURST-coslp-MQMAS spectra with (a) z-filter and (b) full-echo (τ_{echo} = 0.3 ms) acquisitions. RD = 0.5 s, T_{exp} = 1.0 h each. On each spectrum the intensity is given relative to that observed with DQF-STMAS. **hp-MQMAS/DQF-STMAS**: NS = 96 (Z), 192 (FE), Δ_{t1} = {16/32} μs, N_{t1} = 70 (Z), 35 (FE), ν_1 {p1, p2, p3, p4} = {100, 100, 20, 20} kHz. **WURST-lp-MQMAS**: ν_1 = 11, ν_{irr} = +230 kHz. **WURST-coslp-MQMAS**: ν_1 = 14, ν_{irr} = 0, ν_{cos} = 200 kHz. **WURST$_{80}$**: τ_{WURST} = 1 ms, ν_{sweep} = ν_R = 62.5, $\nu_{1,WURST}$ = 20, ν_{off} = +400 kHz.

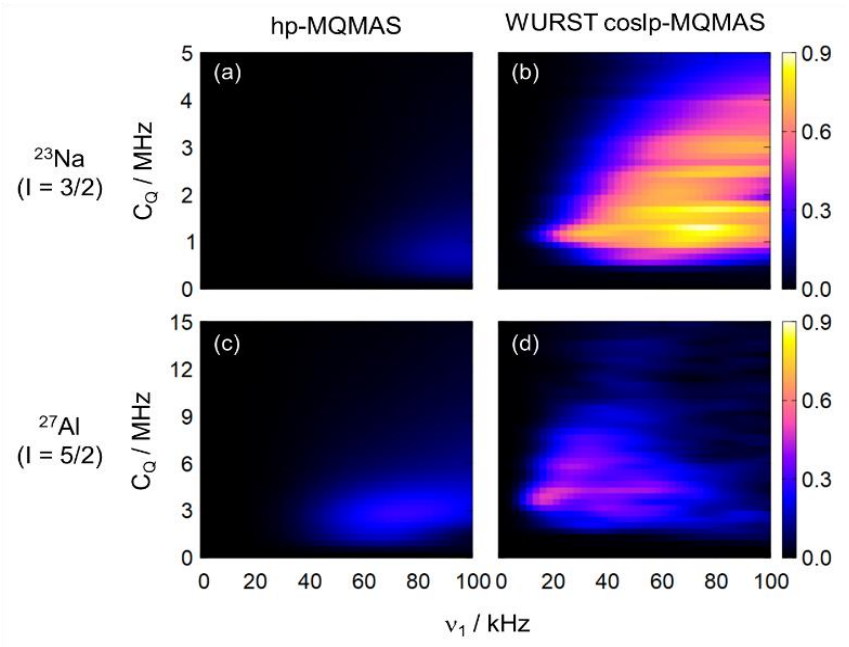

Fig.8. Simulated (a,b) ^{23}Na (I = 3/2) and (c,d) ^{27}Al (I = 5/2) signal intensity of hp-MQMAS and WURST-coslp-MQMAS, with respect to C_Q and the RF-field (ν_1) of the excitation/conversion pulses. **hp-MQMAS**: {p1, p2, p3, p4} μs = {3.5, 3.5, 12.5, 25} for ^{23}Na, {4.0, 1.8, 8, 16} for ^{27}Al, with ν_1 (p3, p4) = 10 kHz. **WURST-coslp-MQMAS**: ν_{cos} = 250 kHz. **WURST$_{80}$**: τ_{WURST} = 1 ms, ν_{sweep} = ν_R = $\nu_{1,WURST}$ = 20, ν_{off} = +300 kHz.